Am J Physiol Heart Circ Physiol 305: H1451–H1461, 2013.
First published September 6, 2013; doi:10.1152/ajpheart.00238.2013.

CALL FOR PAPERS | *Pathophysiology of Hypertension*

COX-1-derived PGE_2 and PGE_2 type 1 receptors are vital for angiotensin II-induced formation of reactive oxygen species and Ca^{2+} influx in the subfornical organ

Gang Wang,[1] Pallabi Sarkar,[2] Jeffrey R. Peterson,[2] Josef Anrather,[1] Joseph P. Pierce,[1] Jamie M. Moore,[1] Ji Feng,[1] Ping Zhou,[1] Teresa A. Milner,[1] Virginia M. Pickel,[1] Costantino Iadecola,[1] and Robin L. Davisson[2,3]

[1]*The Brain and Mind Research Institute, Weill Cornell Medical College, New York, New York;* [2]*Department of Cell and Developmental Biology, Weill Cornell Medical College, New York, New York; and* [3]*Department of Biomedical Sciences, College of Veterinary Medicine, Cornell University, Ithaca, New York*

Submitted 22 March 2013; accepted in final form 4 September 2013

Wang G, Sarkar P, Peterson JR, Anrather J, Pierce JP, Moore JM, Feng J, Zhou P, Milner TA, Pickel VM, Iadecola C, Davisson RL. COX-1-derived PGE_2 and PGE_2 type 1 receptors are vital for angiotensin II-induced formation of reactive oxygen species and Ca^{2+} influx in the subfornical organ. *Am J Physiol Heart Circ Physiol* 305: H1451–H1461, 2013. First published September 6, 2013; doi:10.1152/ajpheart.00238.2013.—Regulation of blood pressure by angiotensin II (ANG II) is a process that involves the reactive oxygen species (ROS) and calcium. We have shown that ANG-II type 1 receptor (AT_1R) and prostaglandin E_2 (PGE_2) type 1 receptors (EP_1R) are required in the subfornical organ (SFO) for ROS-mediated hypertension induced by slow-pressor ANG-II infusion. However, the signaling pathway associated with this process remains unclear. We sought to determine mechanisms underlying the ANG II-induced ROS and calcium influx in mouse SFO cells. Ultrastructural studies showed that cyclooxygenase 1 (COX-1) codistributes with AT_1R in the SFO, indicating spatial proximity. Functional studies using SFO cells revealed that ANG II potentiated PGE_2 release, an effect dependent on AT_1R, phospholipase A_2 (PLA_2) and COX-1. Furthermore, both ANG II and PGE_2 increased ROS formation. While the increase in ROS initiated by ANG II, but not PGE_2, required the activation of the AT_1R/PLA_2/COX-1 pathway, both ANG II and PGE_2 were dependent on EP_1R and Nox2 as downstream effectors. Finally, ANG II potentiated voltage-gated L-type Ca^{2+} currents in SFO neurons via the same signaling pathway required for PGE_2 production. Blockade of EP_1R and Nox2-derived ROS inhibited ANG II and PGE_2-mediated Ca^{2+} currents. We propose a mechanism whereby ANG II increases COX-1-derived PGE_2 through the AT_1R/PLA_2 pathway, which promotes ROS production by EP_1R/Nox2 signaling in the SFO. ANG II-induced ROS are coupled with Ca^{2+} influx in SFO neurons, which may influence SFO-mediated sympathoexcitation. Our findings provide the first evidence of a spatial and functional framework that underlies ANG-II signaling in the SFO and reveal novel targets for antihypertensive therapies.

subfornical organ; angiotensin II; slow-pressor; hypertension; prostaglandins; reactive oxygen species; calcium channel

HYPERTENSION POSES a significant challenge to public health and healthcare by increasing the risk for heart attack, stroke, and kidney failure. The "slow pressor" hypertension, a delayed increase in blood pressure in response to increased systemic angiotensin II (ANG II), is elicited through the subfornical organ (SFO), a small forebrain structure devoid of the blood-brain barrier (6, 22, 41, 49). SFO neurons express ANG-II type 1 receptors (AT_1Rs) and respond to circulating ANG II (11, 22) by sending signals through angiotenergic and glutamatergic projections directly to the paraventricular nucleus (PVN) (3, 11, 13) and other autonomic nuclei that control sympathetic outputs and blood pressure (31). The ANG II-induced upregulation of sympathoexcitation, followed by an elevation of blood pressure, is mediated through reactive oxygen species (ROS) (10, 42, 53, 69) and Ca^{2+} (15, 18, 33). It is well established that ANG II-mediated signals activate NADPH oxidase, leading to accumulation of ROS in the brain that are functionally coupled with hypertensive responses (67). This ANG II-mediated overproduction of ROS is also associated with the activation of voltage-gated L-type Ca^{2+} channels in central neurons (52, 57, 58, 70) and other cell types (2, 55, 62). Activation of L-type Ca^{2+} channels is critical to neurotransmission and long-term potentiation (LTP) in the central nervous system (60, 64).

Previous work has also revealed that the activation of AT_1R results in arachidonic acid (AA) release from membrane phospholipids by phospholipases A_2 (PLA_2) (54). AA is then metabolized to prostaglandin E_2 (PGE_2) by cyclooxygenase-1 (COX-1) or cyclooxygenase-2 (COX-2). Accumulating evidence suggests that COX-derived PGE_2 plays important roles in the regulation of cardiovascular dysfunctions, including ANG II-induced hypertension (4, 6, 21, 39, 40, 45, 56). The PGE_2 receptor subtype 1 (EP_1R) is expressed in the SFO, and studies using genetically modified mice have shown that it plays an important role in signaling the onset of slow-pressor ANG-II hypertension (6, 21). As a member of the G protein-coupled receptor family (17, 25), EP_1R is involved not only in ANG II-elicited ROS production in the SFO (6) but also in the regulation of Ca^{2+} influx through Ca^{2+} channels in neurons and neuroendocrine cells (4, 24, 25, 34). To better understand the complex mechanisms underlying hypertension, it is essential to determine if and how PGE_2, EP_1R, ROS, and Ca^{2+} are functionally linked to serve as key intermediate molecules in ANG II-mediated signaling in SFO neurons.

In this study, we sought to uncover the roles of key prostanoid-linked signals, including PLA_2, COX-1, COX-2, and EP_1R, in ANG II-elicited ROS production and voltage-gated Ca^{2+} influx. Using electron microscopic immunolabeling, we found that COX-1 was coexpressed with AT_1R in SFO neurons. Consistent with this finding, ANG II-triggered PGE_2

Address for reprint requests and other correspondence: G. Wang, The Brain and Mind Research Inst., Weill Cornell Medical College, 407 E. 61st St., Rm. 308, New York, NY 10065 (e-mail: gaw2001@med.cornell.edu).

release from SFO cells was AT_1R and COX-1 dependent. In addition, ANG II induced ROS formation and L-type voltage-gated Ca^{2+} currents (L-VDCCs) via PLA_2, COX-1-derived PGE_2, and EP_1R. Finally, Nox2 was identified as the source of ANG II-induced, EP_1R-mediated ROS production in the SFO.

MATERIALS AND METHODS

Materials. All procedures were approved by the Animal Care and Use Committee at Weill Cornell Medical College. Adult (8–10 wk old) C57Bl/6 wild-type (WT) and transgenic mice, including AT_1R-enhanced green fluorescent protein (eGFP), $EP_1R^{-/-}$, COX-$1^{-/-}$, COX-$2^{-/-}$, and Nox$2^{-/-}$, were obtained from in-house colonies. ANG II, pronase, thermolysin, nifedipine, BAY K 8644, tetrodotoxin (TTX), ω-conotoxin (Ctx)-GVIA, and *N*-(*p*-amylcinnamoyl)anthranilic acid (ACA) were purchased from Sigma-Aldrich (St. Louis, MO). Mn(III)tetrakis(4-benzoic acid)porphyrin chloride (MnTBAP) was procured from EMD Biosciences. PGE_2, SC51089, SC560, and NS398 were obtained from Cayman Chemical (Ann Arbor, MI). The AT_1R antagonist losartan was a gift from the DuPont Merck Pharmaceutical (Deepwater, NJ). The NADPH oxidase polypeptide inhibitor $gp91^{phox}$ docking sequence (gp9-ds) [H]GGGGCSTRIRRQL[NH_2] and the scrambled gp91-ds (s-gp91-ds) with a sequence of [H]GGGGCLRITRQSR[NH_2] were purchased from Bio-Synthesis (Lewisville, TX). Dihydroethidium (DHE) and calcein AM were purchased from Invitrogen (Carlsbad, CA). The COX-1 antibody (M-20, No. sc-1754, an affinity-purified goat antibody raised against the COOH-terminus of mouse COX-1) was purchased from Santa Cruz Biotechnology (Santa Cruz, CA), and the GFP antibody (GFP-1020, a chicken antibody) was purchased from Aves Laboratories (Tigard, OR).

Electron microscopy. Tissue was processed and analyzed as previously described (19, 43). In brief, three males of AT_1R-eGFP and WT age-matched mice were anesthetized with pentobarbital sodium, and their brains were fixed by perfusion with heparin-saline (1,000 U/ml), followed consecutively by 3.8% acrolein (Polysciences) in 2% paraformaldehyde in 0.1 mol/l phosphate buffer and then 2% paraformaldehyde in phosphate buffer. Coronal 40-μm vibratome sections were cut through the SFO and transferred to a storage solution for storage at −25°C. Random SFO sections were incubated for 48 h (24 h at room temperature, and 24 h at 4°C) in 0.1 mol/l Tris-buffered saline-0.1% bovine serum albumin solution containing either *1*) a cocktail of the COX-1 antibody [1:150, for immunogold (ImG) labeling] and the GFP antibody [1:2,500, for immunoperoxidase (ImP) labeling] for double labeling or *2*) the COX-1 antibody (1:2,000, for ImP labeling) for single labeling. Sections were then placed for 30 min in either biotinylated secondary donkey anti-chicken or anti-goat IgG (1:400, Jackson), and avidin-biotin peroxidase complex (ABC Elite Kit, Vector). Bound peroxidase was visualized with 3,3′-diaminobenzidine (Sigma-Aldrich) and hydrogen peroxide (H_2O_2). Tissue processed for dual immunolabeling was additionally incubated overnight in a 1-nm gold particle-conjugated donkey anti-goat secondary IgG (1:50, EMS), followed by postfixation in 2% glutaraldehyde (10 min) and silver intensification using an IntenSE-M Kit (7 min, Amersham). Sections were then postfixed in 2% osmium tetroxide and embedded in EM bed-812 (EMS). Ultrathin sections (70 nm) containing the SFO were cut and collected onto thin bar copper mesh grids (EMS), and counter stained with uranyl acetate and Renyold's lead citrate before examination on a Philips CM10 Technai electron microscope (FEI Company). To quantify COX-1 ImG labeling, undamaged regions of neuropil adjacent to the plastic/tissue interface (i.e., near to the tissue surface) in randomly selected grid square fields, in central portions of the SFO, were examined. In two grids from each AT_1R-eGFP animal, all ImG particles in such fields were categorized in terms of *1*) the type of ultrastructural process they were associated with, in neurons (i.e., soma, dendrite, terminal, and axon), glia, and vascular glia (associated with fenestrated capillaries or vascular epithelial cells) and *2*) whether that process also contained AT_1R-eGFP ImP labeling.

Enzymatic dissociation of cells from the SFO and the PVN tissues. The brain was quickly removed and transferred to a chamber containing ice-cold sucrose-artificial cerebrospinal fluid composed of (in mmol/l) 26 $NaHCO_3$, 1 NaH_2PO_4, 3 KCl, 5 $MgSO_4$, 0.5 $CaCl_2$, 10 glucose, and 248 sucrose, oxygenated with 95% O_2-5% CO_2 (pH 7.4). Coronal section of 300 μm in thickness were obtained using Leica VT1000s vibratome (Leica Microsystems) and stored in a custom-designed chamber containing lactic acid-artificial cerebrospinal fluid (l-aCSF) composed of (in mmol/l): 124, NaCl; 26, $NaHCO_3$; 5, KCl; 1, NaH_2PO_4; 2, $MgSO_4$; 2, $CaCl_2$; 10, glucose; 4.5, lactic acid; oxygenated with 95% O_2 and 5% CO_2, pH 7.4. The location of the SFO is characterized by its dorsal connection with the hippocampal commissure, protruding into the third ventricle of the brain. The brain section containing the SFO was put under a dissection light microscope. The SFO tissue (~450 μm in diameter) was quickly punched out and placed in oxygenated l-aCSF containing 0.01% thermolysin and 0.01% pronase for enzymatic digestion for 2 h at 33°C. The PVN region was identified using lateral ventricle, fornix, and optic tracts as landmarks. The PVN was punched out under dissection microscope and placed in oxygenated l-aCSF containing 0.01% thermolysin and 0.01% pronase for enzymatic digestion for 2 h at 33°C, followed by washing with l-aCSF and trituration of the digested tissue with only 0.3 ml l-aCSF to obtain cell suspension. The cell suspension was quickly plated on a 35-mm petri dish coated with poly-L-lysin for 5–8 min before starting perfusion with oxygenated l-aCSF. Calcein AM (1 μmol/l), a nonfluorescent and cell permeant compound that is hydrolyzed by intracellular esterases into the fluorescent anion calcein, was used to test the viability of isolated SFO cells (44) following enzymatic dissociation.

PGE_2 assay. WT, COX-$1^{-/-}$, or COX-$2^{-/-}$ mice were euthanized, and the SFO and PVN tissues were collected from mice (2 SFO tissues per biological sample). The dissociated SFO cells were obtained by enzymatic digestion, as described above. Each sample was pretreated with vehicle or ANG II (100 nmol/l) and various chemical modulators for 30 min before its supernatant was extracted for detection of PGE_2 concentration using an EIA kit (Cayman Chemical).

ROS detection. Intracellular ROS levels in dissociated SFO cells were assessed using DHE. SFO cells were dissociated as described above, moved to a petri dish mounted on Nikon diaphot 300 inverted microscope (Nikon, Japan), and incubated with DHE (2 μmol/l) for 30 min. The fluorescence intensity was measured before (vehicle) and after application of ANG II or PGE_2 using an ethidium bromide (DNA complex) filter (Chroma Technology, Bellows Falls, VT) with the spectrum of an excitation maximum 510 nm and an emission maximum 605 nm, which indicates the presence of superoxide (O_2^-) and possibly other ROS such as H_2O_2, hydroxyl radical, and peroxynitrite (47). To validate ROS measurement using this system, we tested the capability of exogenous H_2O_2 to increase DHE signal in the SFO cells. The increase in DHE-derived fluorescence observed after treatment of SFO cells with H_2O_2 is attributed to intracellular stimulation of superoxide production by H_2O_2 (65). Addition of H_2O_2 (30 and 300 μmol/l) to the dissociated SFO cells did increase DHE signal in a dose-dependent manner (data not shown here). Data are expressed as DHE fluorescence intensity relative to control samples (Ft/Fo).

Whole cell-patch recording. The dissociated SFO cells were placed in a 35-mm petri dish mounted on the Nikon inverted microscope and perfused with the oxygenated l-aCSF at room temperature (24–26°C). The whole cell-patch recording of isolated SFO neurons was performed using an Axopatch-200A patch-clamp amplifier (Molecular Devices) and a glass electrode pulled by a P-97 micropipette puller (Sutter Instruments) with tip resistance of 3–5 MΩ when filled with a pipette solution containing (in mmol/l) 145 Cs-gluconate, 17 CsCl, 5 EGTA, 1 $MgCl_2$, 10 HEPES, 2 ATP, and 0.2 cAMP (pH 7.3). Series resistance and membrane capacitance were compensated. Bipolar

SFO neurons were visualized following dissociation. TTX-sensitive voltage-gated Na^+ currents were recorded to confirm that the patched cell was a neuron. Two millimole/liter Ca^{2+} in l-aCSF was used as a charge carrier for the voltage-gated Ca^{2+} currents elicited by a 500-ms depolarization pulse from a holding potential at −60 mV to stepping potentials between −50 and +20 mV. To selectively record the long-lasting (L)-type Ca^{2+} current, the selective voltage-gated Na^+ channel blocker TTX (1 μmol/l) and N-type Ca^{2+} channel blocker Ctx-GVIA (1 μmol/l) were added to the perfusion buffer in some patched SFO neurons. The amplitude of L-VDCC was measured at the end of 500-ms pulse (57, 58). The amplitudes of Ca^{2+} currents were analyzed using pClamp 8 (Molecular Devices, Sunnyvale, CA).

Data analysis. Data are expressed as means ± SE. Multiple comparisons were evaluated by ANOVA, followed by post hoc analysis using Tukey's test with paired comparison. Differences were considered statistically significant at $P < 0.05$.

RESULTS

COX-1 is coexpressed with AT$_1$R in SFO neurons. The SFO contains a network of diversified neurons, neuronal processes, and glial cells. To establish a structural framework from which to best unravel key functional interactions, we performed ultrastructural labeling of COX-1 and AT$_1$R within the SFO. Examination of central portions of the SFO revealed that COX-1 ImG labeling was common and was concentrated in postsynaptic neuronal processes and glial processes (Fig. 1). Quantification of this distribution pattern (Fig. 1*D*) demonstrated that 60% of the ImG particles were associated with either neuronal somata or dendrites, and 30% were associated with glial processes in the neuropil (total number of ImG particles examined, 1,072). In addition, 68% of the COX-1 ImG-labeled postsynaptic neuronal processes (i.e., somal and dendritic) also displayed AT$_1$R-eGFP ImP labeling. The results confirm that AT$_1$R and COX-1 are spatially linked and provide anatomical support for the theory that COX-1 may be associated with ANG II-elicited generation of PGE_2 in SFO neurons.

ANG II-triggered endogenous PGE_2 release from dissociated SFO cells is dependent on AT$_1$R, PLA$_2$, and COX-1. Following dissociation of SFO cells, calcein AM (1 μmol/l) was loaded to isolated cells to check viability. As shown in Fig. 2*A*, one example of calcein-labeling of dissociated SFO cells lasted 1 h, indicating viability of the in vitro model. In addition, the time course of calcein-labeled SFO cells also indicates that most

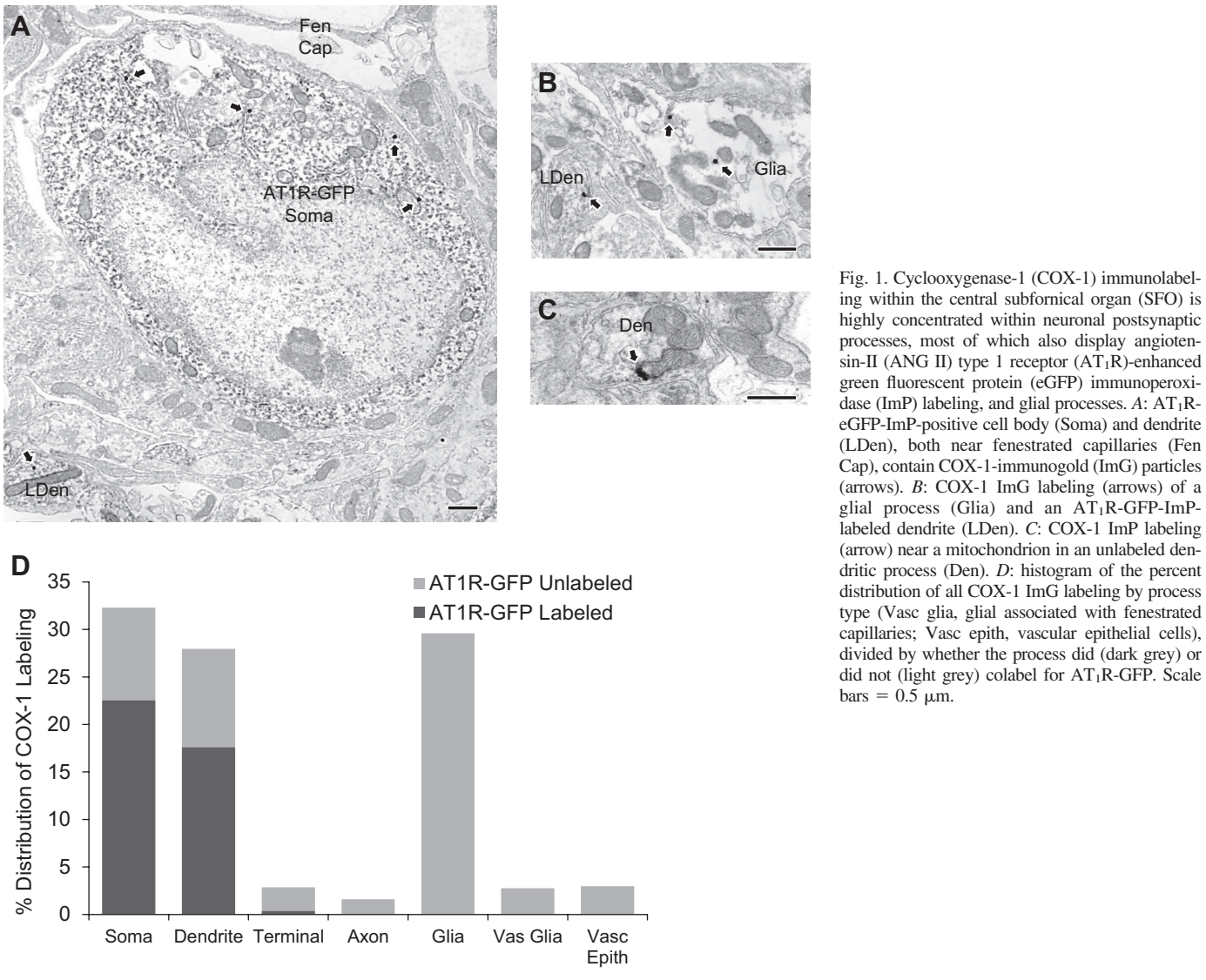

Fig. 1. Cyclooxygenase-1 (COX-1) immunolabeling within the central subfornical organ (SFO) is highly concentrated within neuronal postsynaptic processes, most of which also display angiotensin-II (ANG II) type 1 receptor (AT$_1$R)-enhanced green fluorescent protein (eGFP) immunoperoxidase (ImP) labeling, and glial processes. *A*: AT$_1$R-eGFP-ImP-positive cell body (Soma) and dendrite (LDen), both near fenestrated capillaries (Fen Cap), contain COX-1-immunogold (ImG) particles (arrows). *B*: COX-1 ImG labeling (arrows) of a glial process (Glia) and an AT$_1$R-GFP-ImP-labeled dendrite (LDen). *C*: COX-1 ImP labeling (arrow) near a mitochondrion in an unlabeled dendritic process (Den). *D*: histogram of the percent distribution of all COX-1 ImG labeling by process type (Vasc glia, glial associated with fenestrated capillaries; Vasc epith, vascular epithelial cells), divided by whether the process did (dark grey) or did not (light grey) colabel for AT$_1$R-GFP. Scale bars = 0.5 μm.

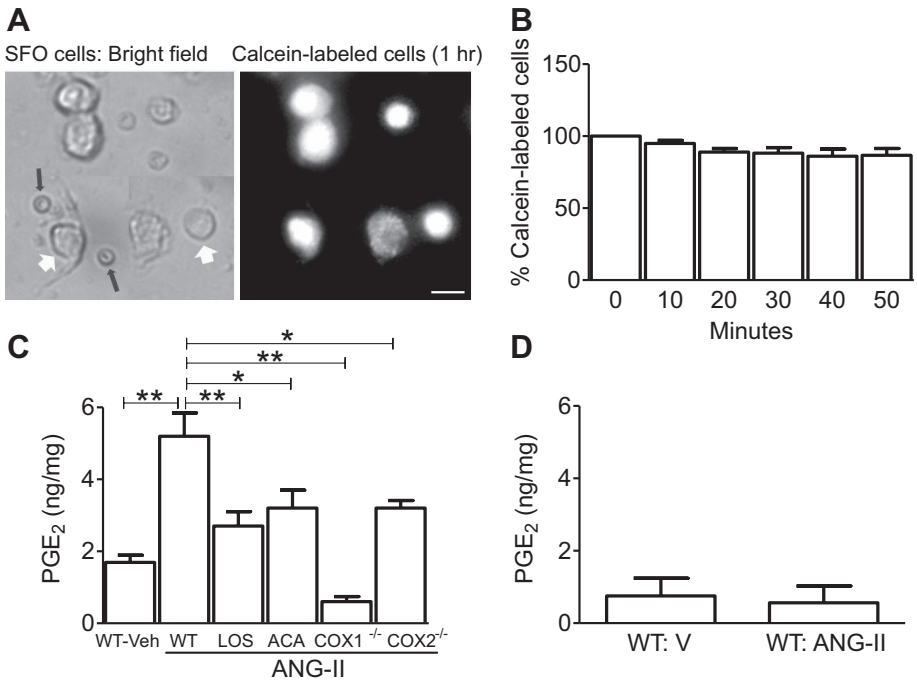

Fig. 2. *A*: one example of calcein-labeled isolated SFO cells 1 h after loading calcein AM (1 μmol/l). The white arrows indicate SFO neurons, whereas black arrows indicate red blood cells. Bar = 10 μm. *B*: time course of a group of calcein-labeled SFO cells is shown ($P > 0.05$ vs. 0 min, number of experiments = 3; cell number in each experiment = 48–54). *C*: histogram shows amounts of endogenous prostaglandin E_2 (PGE_2) released from the wild-type (WT) SFO cells in the presence of vehicle (Veh, $N = 9$), ANG II (100 nmol/l, $N = 5$), coapplied AT_1R antagonist losartan (Los, 3 μmol/l, $N = 9$) and the phospholipase A_2 (PLA_2) inhibitor *N*-(*p*-amylcinnamoyl)anthranilic acid (ACA; 1 μmol/l, $N = 8$) or endogenous PGE_2 released from COX-$1^{-/-}$ ($N = 6$) and COX-$2^{-/-}$ ($N = 5$) SFO cells in the presence of ANG II (100 nmol/l), respectively. *D*: histogram summarizes amounts of endogenous PGE_2 released from WT paraventricular nucleus cells in the presence of Veh (V; $N = 4$) and ANG II (100 nmol/l, $N = 4$). Each tissue sample was collected from 2 mice. *$P < 0.05$ vs. WT SFO vehicle; **$P < 0.01$ vs. WT SFO vehicle.

isolated SFO cells, including neurons, remained viable following 50 min of calcein labeling (86.7 ± 4.7%, $P > 0.05$ vs. 0 min, cell number from each experiment = 48–54, number of experiments = 3) (Fig. 2*B*). Taken together, this proved the viability of the isolated SFO cells and neurons and allowed us to perform further functional studies in vitro.

Considering that COX-1 was present in SFO neurons, often in the same cells as AT_1R, we sought to determine whether ANG II would elicit PGE_2 production from dissociated SFO cells and, if so, what pathway might be involved in the PGE_2 release (6, 29, 54). As shown in Fig. 2*C*, the basal amount of endogenous PGE_2 released from WT SFO cells following incubation in vehicle for 30 min was 1.69 ± 0.2 ng/mg ($N = 9$). Incubation in ANG II (100 nmol/l) for 30 min elicited a significant increase in endogenous PGE_2 release from WT SFO cells (+208 ± 38.5%, $P < 0.01$ vs. WT SFO vehicle, $N = 5$). This effect was blunted when the cells were preincubated with the AT_1R antagonist losartan (3 μmol/l, 58.8 ± 23.5%, $P > 0.05$ vs. WT SFO vehicle, $N = 9$) or the PLA_2 antagonist ACA (1 μmol/l, 88.2 ± 29.4%, $P > 0.05$ vs. WT SFO vehicle, $N = 8$). Furthermore, incubation of COX-$1^{-/-}$ SFO cells in ANG II did not increase PGE_2 release (−64.5 ± 8.3%, $P > 0.05$ vs. WT SFO vehicle, $N = 6$). Incubation of COX-$2^{-/-}$ SFO cells in ANG II partially but significantly inhibited PGE_2 release (+89.4 ± 12.4%, $P < 0.05$ vs. WT SFO vehicle, $N = 5$). As shown in Fig. 2*D*, the basal levels of endogenous PGE_2 released from WT PVN cells following incubation in vehicle and ANG II (100 nmol/l) were relatively low compared with WT SFO cells (vehicle, 0.75 ± 0.49 ng/mg $N = 4$; and ANG II, 0.57 ± 0.47 ng/mg; $P > 0.05$, $N = 4$). These results indicate that ANG II elicits endogenous PGE_2 release from SFO cells, and this PGE_2 production may be dependent on the conversion of AA by COX-1. Importantly, this provides mechanistic support for our previous finding that COX-1-dependent PGE_2 formation plays a key role in ANG II-induced hypertension in the SFO.

ANG II and PGE_2 induce increased ROS production in SFO cells. It has been established that the SFO mediates systemic ANG II-dependent hypertension via increased production of ROS (6, 66, 68). Moreover, we have recently reported that a single dose (100 nmol/l) of ANG II causes a significant increase in ROS formation in WT SFO cells in vitro, a response that was absent in either $EP_1R^{-/-}$ or COX-$1^{-/-}$ SFO cells, but was intact in COX-$2^{-/-}$ SFO cells (6). Using the EP_1R antagonist SC51089, we also confirmed that ANG II-induced ROS formation in WT SFO cells was via EP_1R. In addition, PGE_2 (100 nmol/l) elicited increases in ROS formation to a similar extent as ANG II (6). These data indicate that PGE_2, via EP_1R, serves as a downstream signal in ANG II-induced ROS formation. Using DHE as a fluorescence ROS indicator, we thus focused on the roles of other critical elements in ANG-II signaling pathway, including AT_1R, PLA_2, and NADPH oxidase, in ANG II- and PGE_2-induced ROS formation in SFO cells.

As shown in Fig. 3, both exogenous ANG II ($N = 8$–24 per individual dose) and PGE_2 ($N = 6$–18 per individual dose) increased the DHE signal in a dose-dependent manner in dissociated WT SFO cells. Coapplication of the AT_1R antagonist losartan (3 μmol/l) significantly inhibited the increase in DHE induced by ANG II, but not by PGE_2 (Fig. 3, *B* and *C*).

As shown in Fig. 4, ANG II (100 nmol/l) induced an increase in DHE signal (+25 ± 3%, $P < 0.01$ vs. vehicle, $n = 9$), a response that was blocked by the general PLA_2 inhibitor ACA (1 μmol/l), the COX-1 inhibitor SC560 (10 μmol/l), the NADPH oxidase peptide inhibitor gp91-ds (1 μmol/l) and in Nox$2^{-/-}$ cells (Fig. 4*A*), but not by s-gp91-ds. PGE_2 (100 nmol/l) also induced a similar increase in ROS formation (+32 ± 8.2%, $P < 0.01$ vs. vehicle, $n = 7$) that was blocked by gp91-ds (1 μmol/l) and in Nox$2^{-/-}$ cells. This effect, however, was not blocked by ACA (1 μmol/l), SC560 (10 μmol/l), or s-gp91-ds (Fig. 4*B*). Taken together, these results indicate that PLA_2-mediated PGE_2 production is downstream of AT_1R but upstream of COX-1 and that

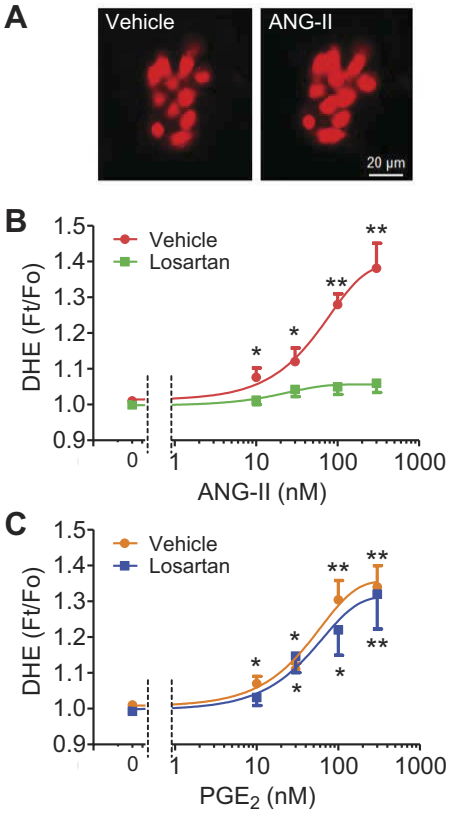

Fig. 3. *A*: representative dihydroethidium (DHE) images of the dissociated WT SFO cells are shown in the presence of vehicle and 100 nmol/l ANG II. *B* and *C*: dose-response curves show effects by ANG II (N of cells = 8–24/each dose; and N of experiments = 5) and PGE_2 (N of cells = 6–18/each dose; and N of experiments = 4) on the relative intensity of DHE in the presence of Veh and the AT_1R antagonist Los (3 μmol/l) in WT SFO cells. *$P < 0.05$ vs. Veh; **$P < 0.01$ vs. Veh.

Nox2 is the source of ANG II and PGE_2-induced ROS formation in SFO cells.

ANG II potentiates the L-VDCC in SFO neurons via AT$_1$R. In addition to generation of ROS, the AT_1R is also involved in voltage-dependent Ca^{2+} influx in the central nervous system (58, 70). Since the L-VDCC is a key signal for the regulation of short- and long-term potentiation and neurotransmitter release (12, 16, 46, 60, 64), we next sought to determine whether the AT_1R-mediated signals were linked with the L-VDCC in SFO neurons. The VDCC in the mouse SFO neurons are composed of transient fast-inactivating and slowly inactivating components (59). Representative traces show that following application of TTX (1 μmol/l) to block voltage-gated Na^+ currents and Ctx-GVIA (1 μmol/l) to inhibit the transient, fast inactivating N-type Ca^{2+} currents in SFO neurons, the L-VDCCs were well distinguished (Fig. 5*A*). Biophysically, the current-voltage curves of this L-VDCC show that it was maximally elicited by a depolarization pulse from the holding potential at −60 mV to the stepping potential at −10 mV (Fig. 5*B*). Pharmacologically, it was activated by ANG II (100 nmol/l), which is in agreement with previous observation in the SFO (61) and other central neurons (Wang et al. 2004). Such effect was attenuated by coapplied losartan (3 μmol/l) (Fig. 5, *A* and *C*). However, further coapplication of the L-type Ca^{2+} channel activator BAY K 8644 (2 μmol/l, $P < 0.01$ vs. vehicle, $N = 16$) restored increased currents, but the L-VDCC was completely inhibited by the L-type Ca^{2+} channel blocker nifedipine (2 μmol/l, $P < 0.01$ vs. vehicle, $N = 6$) (Fig. 5, *A* and *C*) and nonselective Ca^{2+} channel blocker Cd^{2+} (100 μmol/l, $P < 0.01$ vs. vehicle, $N = 6$) (12, 58) (Fig. 5*C*). Taken together, ANG II (100 nmol/l) triggered a potentiation of the L-VDCC in SFO neurons (+53.3 ± 5.8%, $P < 0.01$ vs. vehicle, $N = 9$), a response that was blocked by the AT_1R antagonist losartan (3 μmol/l; −15.7 ± 7.3%, $P < 0.05$ vs. vehicle, $N = 9$) (Fig. 5*C*). These results indicate that ANG II-elicited potentiation of the dihydropyridine-sensitive L-VDCC in SFO neurons is mediated by AT_1R.

PLA$_2$, COX-1, and EP$_1$R are involved in ANG II-induced L-VDCC in SFO neurons. Since the EP_1R is also involved in presynaptic Ca^{2+} influx (24) and glutamate release in the central nervous system (4), we used pharmacological and electrophysiological approaches to determine whether the PLA_2/COX-1/EP_1R signaling molecules that link to ANG II-induced ROS generation also play a role in the ANG II-mediated potentiation of L-VDCC in SFO neurons. As shown in Fig. 6, *A* and *B*, ANG II (100 nmol/l)-induced enhancement of L-VDCC ($P < 0.01$ vs. vehicle, $N = 11$) was abolished by pretreatment with the general PLA_2 inhibitor ACA (1 μmol/l, $P > 0.05$ vs. vehicle, $N = 5$), coapplication of the COX-1 inhibitor SC560 (10 μmol/l, $P > 0.05$ vs. vehicle, $N = 6$), and the EP_1R antagonist SC51089 (10 μmol/l, $P > 0.05$ vs. vehicle, $N = 11$) but were unaffected by coapplication of the COX-2 inhibitor NS398 (10 μmol/l, $P < 0.01$ vs. vehicle, $N = 5$). Moreover, ANG II-induced potentiation in

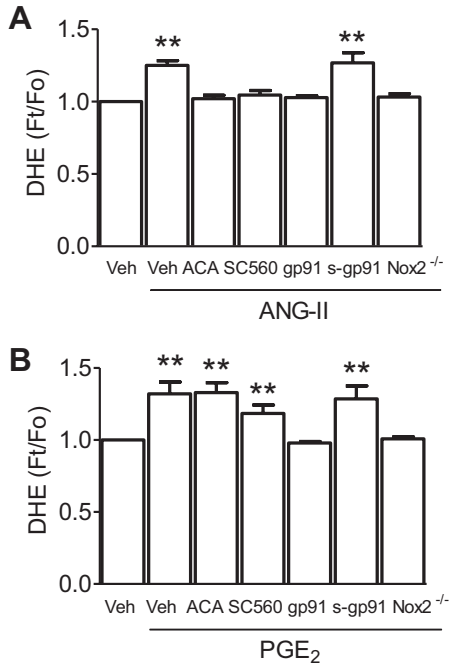

Fig. 4. *A*: histogram shows the relative intensity of DHE in the presence of 100 nmol/l ANG II ($N = 9$) and coapplied ACA (1 μmol/l, $N = 17$), SC560 (10 μmol/l, $N = 26$), gp91-ds-tat (1 μmol/l, gp91, $N = 8$), and scrambled gp91-ds (1 μmol/l, s-gp91, $N = 22$) in WT SFO cells and in Nox2$^{-/-}$ SFO cells ($N = 18$) in the presence of ANG II (100 nmol/l). *B*: histogram summarizes the relative intensity of DHE in the presence of 100 nmol/l PGE_2 ($N = 7$) and coapplied ACA (1 μmol/l, $N = 17$), SC560 (10 μmol/l, $N = 7$), gp91-ds-tat (1 μmol/l, gp91, $N = 9$), and scrambled gp91-ds-tat (1 μmol/l, s-gp91, $N = 20$) in WT SFO cells and in Nox2$^{-/-}$ SFO cells in the presence of PGE_2 (100 nmol/l) ($N = 18$). **$P < 0.01$ vs. Veh.

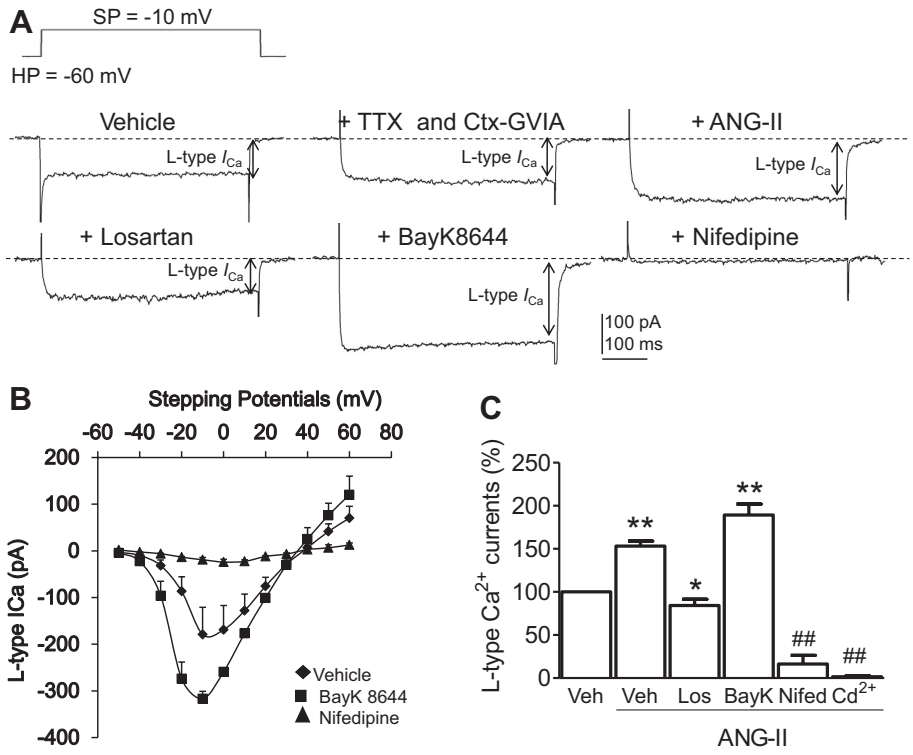

Fig. 5. *A*: representative traces shows L-type voltage-gated Ca^{2+} current (I_{Ca}; L-VDCC) recorded from a WT SFO neuron following applications of Veh, the Na^+ channel blocker tetrodotoxin (TTX; 1 μmol/l), and N-type Ca^{2+} channel blocker ω-conotoxin (Ctx)-GVIA (1 μmol/l), ANG II (100 nmol/l), the AT_1R antagonist Los (10 μmol/l), the selective L-VDCC activator BAY K 8644 (BayK; 2 μmol/l), and the selective L-VDCC blocker nifedipine (Nifed; 2 μmol/l). SP, stepping potential; HP, holding potential. *B*: current-voltage curve of L-VDCC recorded from 4 WT SFO neurons in the presence of Veh, BayK (2 μmol/l), and Nifed (2 μmol/l). *C*: histogram summarizes percent changes in the amplitude of L-VDCC in the presence of Veh ($N = 16$), ANG II (10 μmol/l, $N = 9$), coapplied Los (3 μmol/l, $N = 9$), BayK (2 μmol/l, $N = 16$), Nifed (2 μmol/l, $N = 6$), and Cd^{2+} (100 μmol/l, $N = 6$). ##$P < 0.01$ vs. Veh, ANG II, Los, and BayK; *$P < 0.05$ vs. Veh; **$P < 0.01$ vs. Veh.

L-type Ca^{2+} currents was abolished in $EP_1R^{-/-}$ SFO neurons ($P > 0.05$ vs. vehicle, $N = 7$) (Fig. 6*B*). Figure 6*C* shows the time course of ANG II-induced enhancement in the amplitude of L-VDCC currents in one single isolated SFO neuron. The ANG II-enhanced L-VDCC was reversed by the coapplied EP_1R antagonist SC51089 (10 μmol/l) (Fig. 6*C*). These results establish that PLA_2, COX-1, and EP_1R act downstream of ANG II for potentiation of L-VDCC in SFO neurons.

Nox2-derived ROS contribute to ANG II-induced L-VDCC in SFO neurons. We next we sought to determine the molecular factor responsible for L-VDCC activation and its subcellular localization. Since ROS are known modulators of L-VDCC and they are downstream of the ANG-II signaling pathway, we were curious as to whether Nox2-derived ROS are involved in ANG II-induced L-type Ca^{2+} influx. We examined the effects of the ROS scavenger MnTBAP and $Nox2^{-/-}$ SFO neurons on ANG II-elicited L-VDCC. As shown in Fig. 7*A*, ANG II-induced potentiation in L-VDCC in WT SFO neurons ($P < 0.01$ vs. vehicle, $N = 6$) was abolished by pretreatment with MnTBAP (100 μmol/l, $P > 0.05$ vs. vehicle, $N = 6$). This response was also abolished in $Nox2^{-/-}$ SFO neurons ($P > 0.05$ vs. vehicle, $N = 4$), implying that Nox2-derived ROS are

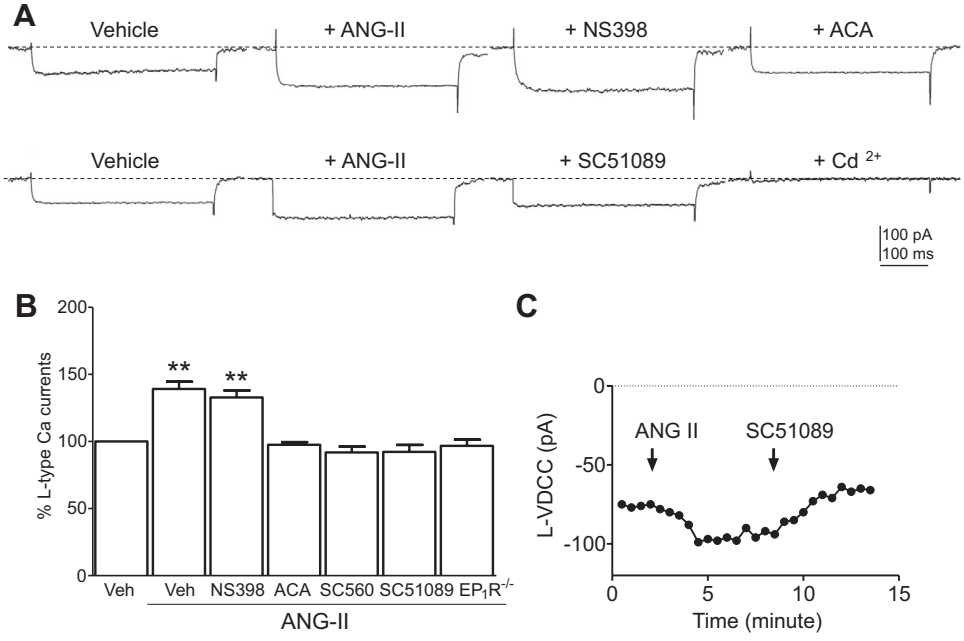

Fig. 6. *A*, *top*: representative traces show L-VDCC recorded from an isolated WT SFO neuron following applications of Veh, ANG II (100 nmol/l), coapplied COX-2 inhibitor NS398 (10 μmol/l), and the PLA_2 inhibitor ACA (1 μmol/l). *A*, *bottom*: representative traces show L-VDCC recorded from another isolated WT SFO neuron following applications of Veh, ANG II (100 nmol/l), coapplied PGE_2 type 1 receptor (EP_1R) antagonist SC51089 (10 μmol/l), and L-VDCC blocker Cd^{2+} (100 μmol/l). *B*: histogram summarizes percent changes in the amplitude of L-VDCC in the presence of Veh, ANG II (100 nmol/l, $N = 11$), coapplied NS398 (10 μmol/l, $N = 5$), ACA (1 μmol/l, $N = 5$), SC560 (10 μmol/l, $N = 6$), SC51089 (10 μmol/l, $N = 11$) in WT SFO neurons, or L-VDCC in $EP_1R^{-/-}$ ($N = 7$) SFO neurons in presence of ANG II (100 nmol/l). **$P < 0.01$ vs. Veh. *C*: time course of the amplitude of L-VDCC recorded from 1 single isolated SFO neuron before and after application of ANG II and coapplied EP_1R antagonist SC51089.

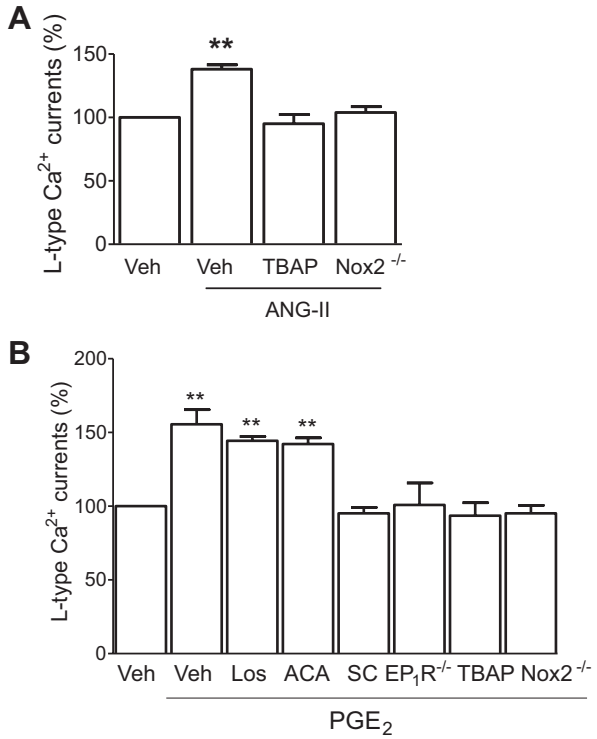

Fig. 7. *A*: histogram summarizes percent changes in the amplitude of L-VDCC in the presence of Veh ($N = 6$), ANG II (100 nmol/l, $N = 6$), coapplied reactive oxygen species scavenger Mn(III)tetrakis(4-benzoic acid)porphyrin chloride (MnTBAP, TBAP; 100 μmol/l, $N = 6$) in WT SFO neurons, or L-VDCC in Nox2$^{-/-}$ neurons ($N = 4$). $^{**}P < 0.01$ vs. Veh. *B*: histogram shows percent changes in the amplitude of L-VDCC in the presence of vehicle (Veh, $N = 16$), PGE_2 (100 nmol/l, $N = 16$), coapplied AT_1R antagonist Los (10 μmol/l, $N = 4$), PLA_2 inhibitor ACA (1 μmol/l, $N = 5$), SC51089 (10 μmol/l, SC, $N = 7$) and MnTBAP (100 μmol/l, $N = 5$), or in EP$_1$R$^{-/-}$ neurons ($N = 5$), and in Nox2$^{-/-}$ SFO neurons ($N = 5$) in the presence of PGE_2 (100 nmol/l). $^{**}P < 0.01$ vs. Veh.

required for the ANG-II potentiation of L-VDCC in SFO neurons.

PGE_2 potentiates L-VDCC via EP$_1$R and Nox2 in SFO neurons. PGE_2 is known to induce an increase in Ca^{2+} influx in the central nervous system (4, 32). Therefore, we further analyzed whether PGE_2, as a downstream signal of ANG-II pathway, is capable of inducing L-VDCC in SFO neurons and, if so, whether it involves the activation of EP$_1$R/Nox2 pathway. We examined the effect of applying antagonists for AT_1R, PLA_2, and EP$_1$R or deleting EP$_1$R and Nox2 on PGE_2-induced L-VDCC in SFO neurons. As shown in Fig. 7*B*, PGE_2 (100 nmol/l) induced potentiation of L-VDCC in SFO neurons (55.6 ± 9.9%, $P < 0.01$ vs. vehicle, $N = 16$), a response that was unaffected by losartan (3 μmol/l, $P < 0.01$ vs. vehicle, $N = 4$) or ACA (1 μmol/l, $P < 0.01$ vs. vehicle, $N = 5$). However, coapplied SC51089 (10 μmol/l, SC, $N = 7$) or genetic deletion of EP$_1$R ($N = 5$) inhibited L-VDCC enhancement induced by PGE_2 ($P > 0.05$ vs. vehicle) (Fig. 7*B*). Moreover, coapplied MnTBAP (100 μmol/l) or genetic deletion of Nox2 ($N = 5$) also abolished the L-VDCC potentiated by PGE_2 ($P > 0.05$ vs. vehicle) (Fig. 7*B*). These results indicate that the EP$_1$R and Nox2 serve as critical signals linking PGE_2 to L-type Ca^{2+} channels in the SFO.

Paracrine regulation of L-VDCC in SFO neurons by endogenous PGE_2. Our ultrastructural data show that COX-1 labeling is concentrated in postsynaptic neuronal processes in the SFO. Assuming that endogenous PGE_2 derived by postsynaptic COX-1 activates presynaptic EP$_1$R (24), which may be responsible for ANG II-induced potentiation of L-VDCC in isolated SFO neurons, we next sought to investigate whether locally generated PGE_2 derived from COX-1 in neighboring cells potentiates L-VDCC in the patched neuron. Adding SC560 (200 nmol/l) to the pipette buffer to inhibit intracellular COX-1 in the SFO neuron patched via the whole cell configuration (Fig. 8*A*), we found that exogenously applied ANG II (100 nmol/l) still increased L-VDCC ($P < 0.01$ vs. vehicle, $n = 9$). However, this response was blocked by extracellular coapplication of SC51089 (10 μmol/l, $P > 0.05$ vs. vehicle, $n = 6$) (Fig. 8*B*). Further coapplication of BAY K 8644 (2 μmol/l) reversed the inhibition of L-VDCC potentiation ($P < 0.01$ vs. vehicle, $n = 4$) in the same patched neuron, indicating that the L-type Ca^{2+} channels retained their functionality (Fig. 8*B*). These results indicate that endogenous PGE_2 derived from ANG II-activated COX-1 in neighboring SFO cells could exert paracrine action by potentiating L-VDCC through EP$_1$R. This assumption is further supported by our ultrastructural labeling studies that indicate extensive expression of COX-1 in SFO neuronal somata, dendrites, and glial cells.

DISCUSSION

COX-derived prostanoids and other endogenous fatty acid metabolites are involved in a wide variety of biological processes (1, 8, 27, 45, 50) and have been implicated in blood pressure regulation (20, 45). The SFO (11, 14), PGE_2/EP$_1$R signaling (6, 7, 21), ROS (6, 66, 68), and voltage-gated Ca^{2+} channels (37, 52, 70) have each been independently proposed as important mediators in the regulation of hypertension. Here we provide the first in vitro evidence that all of these factors are transductionally linked in ANG II-mediated signaling in the

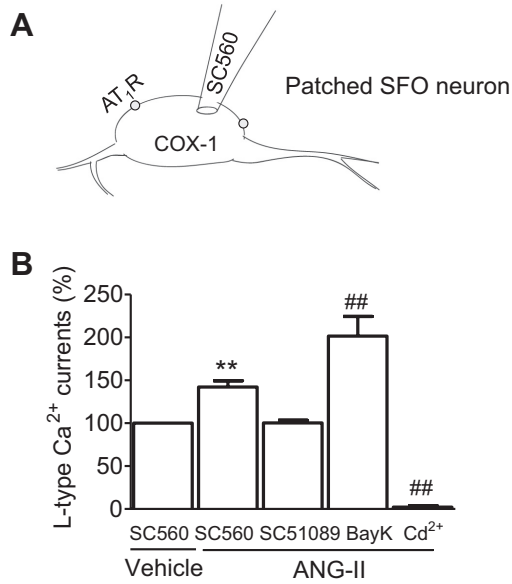

Fig. 8. *A*: schematic illustration of injection of the COX-1 inhibitor SC560 (200 nmol/l) into the patched SFO neuron via the patch electrode. *B*: histogram summarizes percent changes in the amplitude of L-VDCC in SFO neurons intracellularly loaded with SC560 plus extracellularly perfused Veh ($N = 9$), ANG II (100 nmol/l, $N = 9$), coapplied SC51089 (10 μmol/l, $N = 6$), BayK (2 μmol/l, $N = 4$), and Cd^{2+} (100 μmol/l, $N = 4$). $^{**}P < 0.01$ vs. intracellular SC560 plus extracellular Veh; $^{\#\#}P < 0.01$ vs. all other groups.

SFO. We also demonstrate that COX-1 is highly concentrated in neuronal postsynaptic processes in the central SFO, particularly in the processes of cells that coexpress the AT_1R and that COX-1 is the major source for the ANG II-activated PGE_2 release in the SFO. Furthermore, ANG II-evoked PGE_2 and ROS formation in dissociated SFO cells is prevented by deletion of COX-1 and partially attenuated by deletion of COX-2. ANG II or PGE_2-potentiated ROS and Ca^{2+} currents are dependent on PLA_2, EP_1R, and ROS. These results support the notion that COX-1-derived PGE_2 and EP_1R signaling in the SFO are critical for slow-pressor ANG-II hypertension (6) and provide a detailed signaling pathway linking ANG II with ROS and L-VDCC, as summarized schematically in Fig. 9. As previously reported (53, 66), we speculate that this ANG II-induced intracellular increase in O_2^- may also lead to an increase in extracellular H_2O_2. Additionally, the present in vitro data also support the in vivo results recently published by our group (6).

Ultrastructural labeling of SFO neurons supports paracrine action of PGE_2. The neuronal location of AT_1R in the SFO was illustrated by GFP labeling in postsynaptic somata and dendrites, many of which also contained COX-1. The colocalization of AT_1R and COX-1 in the SFO provides valuable ultrastructural support for the functional interaction seen between ANG II and COX-1 in dissociated SFO cells. In dual-labeled somatodendritic profiles, COX-1 ImG labeling was present in the cytoplasmic compartment of SFO neurons. Plasmalemmal labeling of COX-1 was also seen in small- and medium-sized dendrites receiving synaptic input from one or more axon terminals. Postsynaptic coexpression of COX-1 and AT_1R in SFO neurons indicates that COX-1 is likely to be associated with AT_1R-elicited generation of PGE_2 and that release of PGE_2 from postsynaptic sites may modulate EP_1 receptors at presynaptic sites (24). In addition to COX-1, our recent EM data indicate that COX-2 is also present in SFO neurons that express AT_1R (unpublished data).

It is notable that PGE_2 is also produced and released from glial cells (29). Our electron microscopic data demonstrate that processes of glial cells in the SFO express about 30% of the COX-1 ImG labeling, which might also express AT_1R. Furthermore, the fact that inhibition of COX-1 with intracellular SC-560 did not affect ANG II-induced, EP_1R-mediated L-type Ca^{2+} currents in whole cell-patched SFO neurons indicates that COX-1 activation leading to PGE_2 release is of exogenous origin. Thus these data raise the possibility that ANG II triggers PGE_2 release from the neighboring cells, including neurons or glial cells such as ependymal cells, microglia, and astrocytes, and PGE_2 exerts a paracrine action in the SFO.

ANG II, PLA_2, COX-1, and EP_1R-mediated ROS in the SFO. COX-1, PGE_2, and NADPH oxidase-derived oxidative stress are involved in inflammatory responses (63) and EP_1Rs were recently linked to ANG-II hypertension (6, 7). However, if or how these key signaling molecules interacted with one another had not been established. In this study, we found that inhibition of PLA_2, COX-1, and EP_1R prevented ANG II-elicited ROS production in the SFO, raising the possibility that there is molecular cross talk between COX-1/EP_1R and Nox/ROS signaling in SFO neurons. Since the SFO is composed of neurons and nonneuronal glial cells such as ependymal cells, microglia, astrocytes, and vascular cells, ROS production detected in this in vitro study could come from dissociated SFO neurons or glial and vascular cells. However, further investigation is needed to identify different cell types and the exact mechanisms underlying EP_1R-mediated ROS formation via Nox2-NADPH oxidase in the SFO.

EP_1R and Ca^{2+} influx. The role of Nox2-dependent ROS in the regulation of ANG II-potentiated L-type Ca^{2+} currents has been previously addressed in central neurons and other cell types in peripheral tissue (2, 23, 57, 58, 70). However, a link between PGE_2/EP_1R signaling and ANG II-potentiated L-VDCC in central neurons had not been established. Our data provide strong evidence that PGE_2 can potentiate L-VDCC through EP_1R. EP receptors are a family of G protein-coupled receptors that regulate intracellular free Ca^{2+}, and PGE_2 is known to regulate Ca^{2+} influx (4, 5, 25–28, 32, 35, 36) through EP receptors in neurons and other cell types. EP_1R and EP_3R

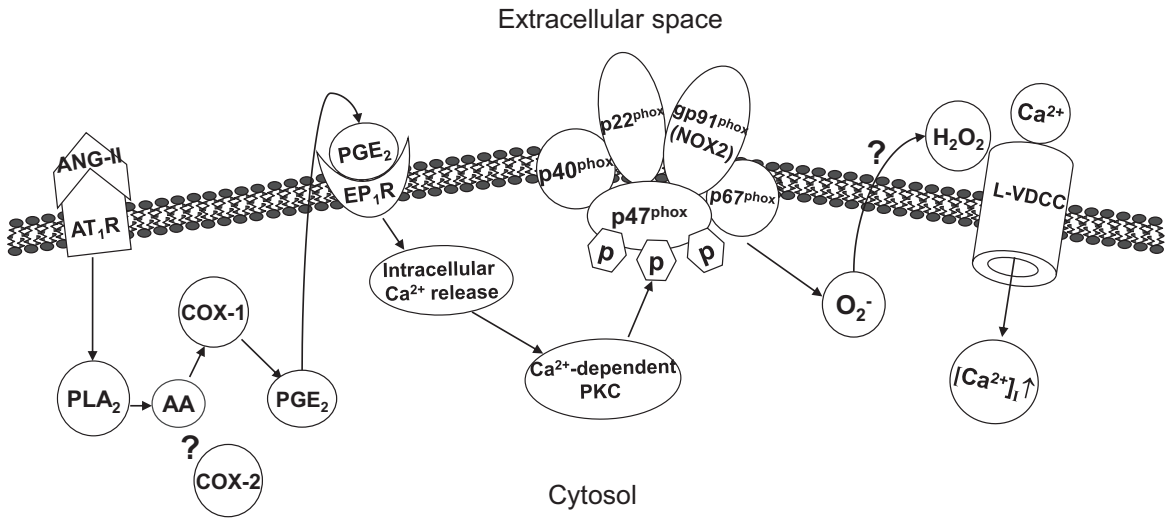

Fig. 9. A summary schematic overview highlights the signaling pathway proposed in the present study. Note: Nox2-containing NADPH oxidase is composed of 5 subunits, the membrane anchored catalytic subunits $gp91^{phox}$ (Nox2) and $p22^{phox}$ and the cytosolic subunits $p47^{phox}$, $p40^{phox}$, and $p67^{phox}$. It is speculated that the intracellular increase in superoxide (O_2^-) leads to an increase in extracellular H_2O_2 (53, 66). P, phosphorylated; AA, arachidonic acid; PKC, protein kinase C; $[Ca^{2+}]_i$, intracellular Ca^{2+} concentration.

couple to $G_{q/11}$ protein and activate phospholipase C (38). However, contrary to potential Ca^{2+}-mobilizing actions by EP_1R, the EP_3R-coupled regulatory effects on Ca^{2+} homeostasis in adrenal medulla chromaffin cells and melanotrophs are inhibitory (25, 36). Nevertheless, because of lack of validated antibodies against EP_1R and selective antagonists for other subtypes of EP receptors, the present study has not ruled in coexpression of AT_1R and EP_1R in the SFO or ruled out the possible involvement of other EP receptor subtypes in the regulation of ANG-II hypertension in this model.

Mechanisms underlying ROS-enhanced gating of L-type Ca^{2+} channels. Our results demonstrate that EP_1R/ROS signaling is required for ANG II and PGE_2 potentiation of L-VDCC in SFO neurons, but EP_1R/ROS signaling is not necessary for direct gating induced by L-type channel activator BAY K 8644. This indicates that ROS has different binding sites from those of BAY K 8644. Recent reports suggest a coupled gating model of L-type isoform $Ca_V1.2$ channel activation by ROS in arterial smooth muscle (2, 37) that provides a novel mechanism for the regulation of Ca^{2+} influx and excitability. Using a TIRF imaging-based approach, a pathway has been characterized that functionally links subplasmalemmal generation of endogenous ROS that precede and colocalize with enhanced L-type Ca^{2+} channel activity via activation of PKCα in cerebral arterial smooth muscle (2). Further studies are needed to determine how ROS are functionally linked to L-VDCC potentiation in the SFO.

Potential contribution of L-type Ca^{2+} currents to SFO function. Though the mechanisms underlying ANG II-induced sympathoexcitation via SFO neuronal projections to other autonomic nuclei remain elusive, it is likely that voltage-gated L-type Ca^{2+} influx is involved in presynaptic glutamate release and therefore synaptic plasticity, such as LTP (16, 46, 64). For LTP mediated by increased release of glutamate in the corticolateral nucleus of the amygdala, L-VDCCs are necessary for the persistent expression, and possibly the induction, of presynaptic cortico-LA LTP. Whereas L-VDCCs only weakly contribute to baseline release, they contribute significantly to increased synaptic transmission (16). On the other hand, the electrical stimulation-induced LTP of synapses onto the excitatory narrow-field vertical neurons of the sSC requires postsynaptic Ca^{2+} elevation by both NMDARs and L-type Ca^{2+} channels during induction but not maintenance (64). Therefore, L-type Ca^{2+} channels might be required for both induction and persistent expression of presynaptic LTP.

The role of SFO L-type voltage-dependent Ca^{2+} channels in ANG II-induced hypertension. The functional link between ANG II and voltage-gated Ca^{2+} influx in central neurons, including sympathetic neurons, has been previously reported (15, 33, 61, 70). In vivo, it is evident that the SFO sends the ANG-II peptidergic efferent to the PVN neurons (13, 30, 31) and that the ANG II-induced hypertension mediated via the SFO is attenuated by intracerebroventricular administration of the L-VDCC blocker nifedipine (48). In vitro, L-VDCC plays an important role in the regulation of peptidergic neurotransmitter release from presynaptic axonal terminals of central neurons (59). Therefore, it can be speculated that AT_1R in SFO sensory neurons are activated by circulating ANG II, which increases Ca^{2+} influx mediated by L-VDCC through EP_1R and ROS pathways. Since increments in intracellular calcium concentration lead to ANG-II release from axonal terminals in the PVN-projecting SFO neurons (18), L-VDCC potentiation may cause excitation of presympathetic neurons in the PVN, leading to hypertension.

Perspective and significance. The in vitro results described here, along with our recently published in vivo results (6), provide strong evidence that EP_1R-mediated ROS formation via Nox2-NADPH oxidase in the SFO may provide useful targets for the treatment of hypertension. SFO-targeted treatment with cytoplasmic superoxide dismutase has proven to be as effective in ameliorating ANG-II hypertension as chronic intracerebroventricular infusion of the AT_1R antagonist losartan (68). Peripheral administration of the AT_1R antagonist losartan may also target the AT_1R expressed in the SFO because of its lack of a normal blood-brain barrier (9). In addition, blocking the ANG-II/PGE2/L-VDCC pathway in the SFO might be beneficial for the treatment of hypertension (51).

In conclusion, the present study used diverse cutting-edge technologies, including electron microscopy, EIA, ROS imaging, patch recording, and null mutant mice to comprehensively determine that ANG II-mediated PLA_2 and PGE_2 signals are coupled with ROS formation and intracellular Ca^{2+} homeostasis in SFO neurons. Additionally, as PGE_2 is also released from glial cells, future studies should focus on the identification of possible distinct contributions by different cell types to ANG II-triggered PGE_2 release. Taken together, our findings are a critical step toward a more complete understanding of ANG-II signaling in the SFO and may provide novel targets for future antihypertensive therapy.

ACKNOWLEDGMENTS

We thank Andreina Gonzalez for assistance with electron microscopic experiments.

GRANTS

This work was supported by National Heart, Lung, and Blood Institute Grants HL-096571, HL-063887, and HL-098351.

DISCLOSURES

No conflicts of interest, financial or otherwise, are declared by the author(s).

AUTHOR CONTRIBUTIONS

G.W., P.S., J.P.P., C.I., and R.L.D. conception and design of research; G.W., P.S., J.R.P., J.A., J.P.P., J.M.M., J.F., P.Z., T.A.M., and R.L.D. performed experiments; G.W., P.S., J.R.P., J.A., J.P.P., J.F., T.A.M., V.M.P., C.I., and R.L.D. analyzed data; G.W., P.S., J.R.P., J.A., J.P.P., V.M.P., C.I., and R.L.D. interpreted results of experiments; G.W., P.S., J.P.P., V.M.P., and R.L.D. prepared figures; G.W., P.S., C.I., and R.L.D. drafted manuscript; G.W., P.S., J.P.P., C.I., and R.L.D. edited and revised manuscript; G.W., P.S., C.I., and R.L.D. approved final version of manuscript.

REFERENCES

1. **Ahmad AS, Yun YT, Ahmad M, Maruyama T, Dore S.** Selective blockade of PGE2 EP1 receptor protects brain against experimental ischemia and excitotoxicity, and hippocampal slice cultures against oxygen-glucose deprivation. *Neurotox Res* 14: 343–351, 2008.
2. **Amberg GC, Earley S, Glapa SA.** Local regulation of arterial L-type calcium channels by reactive oxygen species. *Circ Res* 107: 1002–1010, 2010.
3. **Anderson JW, Smith PM, Ferguson AV.** Subfornical organ neurons projecting to paraventricular nucleus: whole-cell properties. *Brain Res* 921: 78–85, 2001.
4. **Bezzi P, Carmignoto G, Pasti L, Vesce S, Rossi D, Rizzini BL, Pozzan T, Volterra A.** Prostaglandins stimulate calcium-dependent glutamate release in astrocytes. *Nature* 391: 281–285, 1998.

5. **Borgland SL, Connor M, Ryan RM, Ball HJ, Christie MJ.** Prostaglandin E(2) inhibits calcium current in two sub-populations of acutely isolated mouse trigeminal sensory neurons. *J Physiol* 539: 433–444, 2002.
6. **Cao X, Peterson JR, Wang G, Anrather J, Young CN, Guruju MR, Burmeister MA, Iadecola C, Davisson RL.** Angiotensin II-dependent hypertension requires cyclooxygenase 1-derived prostaglandin E2 and EP1 receptor signaling in the subfornical organ of the brain. *Hypertension* 59: 869–876, 2012.
7. **Capone C, Faraco G, Anrather J, Zhou P, Iadecola C.** Cyclooxygenase 1-derived prostaglandin E2 and EP1 receptors are required for the cerebrovascular dysfunction induced by angiotensin II. *Hypertension* 55: 911–917, 2010.
8. **Carlson NG, Rojas MA, Black JD, Redd JW, Hille J, Hill KE, Rose JW.** Microglial inhibition of neuroprotection by antagonists of the EP1 prostaglandin E2 receptor. *J Neuroinflammation* 6: 5, 2009.
9. **Collister JP, Hendel MD.** Role of the subfornical organ in the chronic hypotensive response to losartan in normal rats. *Hypertension* 41: 576–582, 2003.
10. **Datla SR, Griendling KK.** Reactive oxygen species, NADPH oxidases, and hypertension. *Hypertension* 56: 325–330, 2010.
11. **Davisson RL, Oliverio MI, Coffman TM, Sigmund CD.** Divergent functions of angiotensin II receptor isoforms in the brain. *J Clin Invest* 106: 103–106, 2000.
12. **Dolphin AC.** Calcium channel diversity: multiple roles of calcium channel subunits. *Curr Opin Neurobiol* 19: 237–244, 2009.
13. **Ferguson AV.** Angiotensinergic regulation of autonomic and neuroendocrine outputs: critical roles for the subfornical organ and paraventricular nucleus. *Neuroendocrinology* 89: 370–376, 2009.
14. **Ferguson AV, Bains JS.** Actions of angiotensin in the subfornical organ and area postrema: implications for long term control of autonomic output. *Clin Exp Pharmacol Physiol* 24: 96–101, 1997.
15. **Fernandez SF, Huang MH, Davidson BA, Knight PR 3rd, Izzo JL Jr.** Modulation of angiotensin II responses in sympathetic neurons by cytosolic calcium. *Hypertension* 41: 56–63, 2003.
16. **Fourcaudot E, Gambino F, Casassus G, Poulain B, Humeau Y, Luthi A.** L-type voltage-dependent Ca^{2+} channels mediate expression of presynaptic LTP in amygdala. *Nat Neurosci* 12: 1093–1095, 2009.
17. **Furuyashiki T, Narumiya S.** Stress responses: the contribution of prostaglandin E(2) and its receptors. *Nat Rev Endocrinol* 7: 163–175, 2011.
18. **Gebke E, Muller AR, Jurzak M, Gerstberger R.** Angiotensin II-induced calcium signaling in neurons and astrocytes of rat circumventricular organs. *Neuroscience* 85: 509–520, 1998.
19. **Gonzalez AD, Wang G, Waters EM, Gonzales KL, Speth RC, Van Kempen TA, Marques-Lopes J, Young CN, Butler SD, Davisson RL, Iadecola C, Pickel VM, Pierce JP, Milner TA.** Distribution of angiotensin type 1a receptor containing cells in the brains of bacterial artificial chromosome transgenic mice. *Neuroscience* 226: 489–509, 2012.
20. **Grosser T, Fries S, FitzGerald GA.** Biological basis for the cardiovascular consequences of COX-2 inhibition: therapeutic challenges and opportunities. *J Clin Invest* 116: 4–15, 2006.
21. **Guan Y, Zhang Y, Wu J, Qi Z, Yang G, Dou D, Gao Y, Chen L, Zhang X, Davis LS, Wei M, Fan X, Carmosino M, Hao C, Imig JD, Breyer RM, Breyer MD.** Antihypertensive effects of selective prostaglandin E2 receptor subtype 1 targeting. *J Clin Invest* 117: 2496–2505, 2007.
22. **Hendel MD, Collister JP.** Contribution of the subfornical organ to angiotensin II-induced hypertension. *Am J Physiol Heart Circ Physiol* 288: H680–H685, 2005.
23. **Hudasek K, Brown ST, Fearon IM.** H_2O_2 regulates recombinant Ca^{2+} channel alpha1C subunits but does not mediate their sensitivity to acute hypoxia. *Biochem Biophys Res Commun* 318: 135–141, 2004.
24. **Jadhav V, Jabre A, Chen MF, Lee TJ.** Presynaptic prostaglandin E2 EP1-receptor facilitation of cerebral nitrergic neurogenic vasodilation. *Stroke* 40: 261–269, 2009.
25. **Jewell ML, Breyer RM, Currie KP.** Regulation of calcium channels and exocytosis in mouse adrenal chromaffin cells by prostaglandin EP3 receptors. *Mol Pharmacol* 79: 987–996, 2011.
26. **Kaestner L, Tabellion W, Lipp P, Bernhardt I.** Prostaglandin E2 activates channel-mediated calcium entry in human erythrocytes: an indication for a blood clot formation supporting process. *Thromb Haemost* 92: 1269–1272, 2004.
27. **Kawano T, Anrather J, Zhou P, Park L, Wang G, Frys KA, Kunz A, Cho S, Orio M, Iadecola C.** Prostaglandin E2 EP1 receptors: downstream effectors of COX-2 neurotoxicity. *Nat Med* 12: 225–229, 2006.
28. **Kobayter S, Young JS, Brain KL.** Prostaglandin E2 induces spontaneous rhythmic activity in mouse urinary bladder independently of efferent nerves. *Br J Pharmacol* 165: 401–413, 2012.
29. **Leung KH, Chang RS, Lotti VJ, Roscoe WA, Smith RD, Timmermans PB, Chiu AT.** AT1 receptors mediate the release of prostaglandins in porcine smooth muscle cells and rat astrocytes. *Am J Hypertens* 5: 648–656, 1992.
30. **Li Z, Ferguson AV.** Angiotensin II responsiveness of rat paraventricular and subfornical organ neurons in vitro. *Neuroscience* 55: 197–207, 1993.
31. **Li Z, Ferguson AV.** Subfornical organ efferents to paraventricular nucleus utilize angiotensin as a neurotransmitter. *Am J Physiol Regul Integr Comp Physiol* 265: R302–R309, 1993.
32. **Linhart O, Obreja O, Kress M.** The inflammatory mediators serotonin, prostaglandin E2 and bradykinin evoke calcium influx in rat sensory neurons. *Neuroscience* 118: 69–74, 2003.
33. **Ma X, Chapleau MW, Whiteis CA, Abboud FM, Bielefeldt K.** Angiotensin selectively activates a subpopulation of postganglionic sympathetic neurons in mice. *Circ Res* 88: 787–793, 2001.
34. **Marty V, El Hachmane M, Amedee T.** Dual modulation of synaptic transmission in the nucleus tractus solitarius by prostaglandin E2 synthesized downstream of IL-1beta. *Eur J Neurosci* 27: 3132–3150, 2008.
35. **Mochizuki-Oda N, Mori K, Negishi M, Ito S.** Prostaglandin E2 activates Ca^{2+} channels in bovine adrenal chromaffin cells. *J Neurochem* 56: 541–547, 1991.
36. **Nagata T, Harayama N, Sasaki N, Inoue M, Tanaka K, Toyohira Y, Uezono Y, Maruyama T, Yanagihara N, Ueta Y, Shibuya I.** Mechanisms of cytosolic Ca^{2+} suppression by prostaglandin E2 receptors in rat melanotrophs. *J Neuroendocrinol* 15: 33–41, 2003.
37. **Navedo MF, Cheng EP, Yuan C, Votaw S, Molkentin JD, Scott JD, Santana LF.** Increased coupled gating of L-type Ca^{2+} channels during hypertension and Timothy syndrome. *Circ Res* 106: 748–756, 2010.
38. **Nicola C, Timoshenko AV, Dixon SJ, Lala PK, Chakraborty C.** EP1 receptor-mediated migration of the first trimester human extravillous trophoblast: the role of intracellular calcium and calpain. *J Clin Endocrinol Metab* 90: 4736–4746, 2005.
39. **Niwa K, Araki E, Morham SG, Ross ME, Iadecola C.** Cyclooxygenase-2 contributes to functional hyperemia in whisker-barrel cortex. *J Neurosci* 20: 763–770, 2000.
40. **Niwa K, Haensel C, Ross ME, Iadecola C.** Cyclooxygenase-1 participates in selected vasodilator responses of the cerebral circulation. *Circ Res* 88: 600–608, 2001.
41. **Osborn JW, Fink GD, Sved AF, Toney GM, Raizada MK.** Circulating angiotensin II and dietary salt: converging signals for neurogenic hypertension. *Curr Hypertens Rep* 9: 228–235, 2007.
42. **Peterson JR, Burmeister MA, Tian X, Zhou Y, Guruju MR, Stupinski JA, Sharma RV, Davisson RL.** Genetic silencing of Nox2 and Nox4 reveals differential roles of these NADPH oxidase homologues in the vasopressor and dipsogenic effects of brain angiotensin II. *Hypertension* 54: 1106–1114, 2009.
43. **Pierce JP, Kievits J, Graustein B, Speth RC, Iadecola C, Milner TA.** Sex differences in the subcellular distribution of angiotensin type 1 receptors and NADPH oxidase subunits in the dendrites of C1 neurons in the rat rostral ventrolateral medulla. *Neuroscience* 163: 329–338, 2009.
44. **Poole CA, Brookes NH, Clover GM.** Keratocyte networks visualised in the living cornea using vital dyes. *J Cell Sci* 106: 685–691, 1993.
45. **Qi Z, Hao CM, Langenbach RI, Breyer RM, Redha R, Morrow JD, Breyer MD.** Opposite effects of cyclooxygenase-1 and -2 activity on the pressor response to angiotensin II. *J Clin Invest* 110: 61–69, 2002.
46. **Quinlan ME, Alberto CO, Hirasawa M.** Short-term potentiation of mEPSCs requires N-, P/Q- and L-type Ca^{2+} channels and mitochondria in the supraoptic nucleus. *J Physiol* 586: 3147–3161, 2008.
47. **Robinson KM, Janes MS, Pehar M, Monette JS, Ross MF, Hagen TM, Murphy MP, Beckman JS.** Selective fluorescent imaging of superoxide in vivo using ethidium-based probes. *Proc Natl Acad Sci USA* 103: 15038–15043, 2006.
48. **Saad WA, Camargo LA, Guarda IF, Santos TA.** Subfornical organ mediates pressor effect of angiotensin: Influence of nitric oxide synthase inhibitors, AT(1) and AT(2) angiotensin antagonist's receptors. *J Am Soc Hypertens* 2: 326–331, 2008.
49. **Smith PM, Ferguson AV.** Circulating signals as critical regulators of autonomic state–central roles for the subfornical organ. *Am J Physiol Regul Integr Comp Physiol* 299: R405–R415, 2010.
50. **Smyth EM, Grosser T, Wang M, Yu Y, FitzGerald GA.** Prostanoids in health and disease. *J Lipid Res* 50, *Suppl*: S423–S428, 2009.

51. **Takahara A.** Cilnidipine: a new generation Ca channel blocker with inhibitory action on sympathetic neurotransmitter release. *Cardiovasc Ther* 27: 124–139, 2009.
52. **Tolstykh G, de Paula PM, Mifflin S.** Voltage-dependent calcium currents are enhanced in nucleus of the solitary tract neurons isolated from renal wrap hypertensive rats. *Hypertension* 49: 1163–1169, 2007.
53. **Touyz RM.** Reactive oxygen species as mediators of calcium signaling by angiotensin II: implications in vascular physiology and pathophysiology. *Antioxid Redox Signal* 7: 1302–1314, 2005.
54. **Touyz RM, Berry C.** Recent advances in angiotensin II signaling. *Braz J Med Biol Res* 35: 1001–1015, 2002.
55. **Tsai CT, Wang DL, Chen WP, Hwang JJ, Hsieh CS, Hsu KL, Tseng CD, Lai LP, Tseng YZ, Chiang FT, Lin JL.** Angiotensin II increases expression of alpha1C subunit of L-type calcium channel through a reactive oxygen species and cAMP response element-binding protein-dependent pathway in HL-1 myocytes. *Circ Res* 100: 1476–1485, 2007.
56. **Virdis A, Colucci R, Fornai M, Duranti E, Giannarelli C, Bernardini N, Segnani C, Ippolito C, Antonioli L, Blandizzi C, Taddei S, Salvetti A, Del Tacca M.** Cyclooxygenase-1 is involved in endothelial dysfunction of mesenteric small arteries from angiotensin II-infused mice. *Hypertension* 49: 679–686, 2007.
57. **Wang G, Anrather J, Glass MJ, Tarsitano MJ, Zhou P, Frys KA, Pickel VM, Iadecola C.** Nox2, Ca^{2+}, and protein kinase C play a role in angiotensin II-induced free radical production in nucleus tractus solitarius. *Hypertension* 48: 482–489, 2006.
58. **Wang G, Anrather J, Huang J, Speth RC, Pickel VM, Iadecola C.** NADPH oxidase contributes to angiotensin II signaling in the nucleus tractus solitarius. *J Neurosci* 24: 5516–5524, 2004.
59. **Wang G, Dayanithi G, Newcomb R, Lemos JR.** An R-type Ca^{2+} current in neurohypophysial terminals preferentially regulates oxytocin secretion. *J Neurosci* 19: 9235–9241, 1999.
60. **Wankerl K, Weise D, Gentner R, Rumpf JJ, Classen J.** L-type voltage-gated Ca^{2+} channels: a single molecular switch for long-term potentiation/long-term depression-like plasticity and activity-dependent metaplasticity in humans. *J Neurosci* 30: 6197–6204, 2010.
61. **Washburn DL, Ferguson AV.** Selective potentiation of N-type calcium channels by angiotensin II in rat subfornical organ neurones. *J Physiol* 536: 667–675, 2001.
62. **Zeng Q, Han Y, Bao Y, Li W, Li X, Shen X, Wang X, Yao F, O'Rourke ST, Sun C.** 20-HETE increases NADPH oxidase-derived ROS production and stimulates the L-type Ca^{2+} channel via a PKC-dependent mechanism in cardiomyocytes. *Am J Physiol Heart Circ Physiol* 299: H1109–H1117, 2010.
63. **Zhang X, Dong F, Ren J, Driscoll MJ, Culver B.** High dietary fat induces NADPH oxidase-associated oxidative stress and inflammation in rat cerebral cortex. *Exp Neurol* 191: 318–325, 2005.
64. **Zhao JP, Phillips MA, Constantine-Paton M.** Long-term potentiation in the juvenile superior colliculus requires simultaneous activation of NMDA receptors and L-type Ca^{2+} channels and reflects addition of newly functional synapses. *J Neurosci* 26: 12647–12655, 2006.
65. **Zielonka J, Kalyanaraman B.** Hydroethidine- and MitoSOX-derived red fluorescence is not a reliable indicator of intracellular superoxide formation: another inconvenient truth. *Free Radic Biol Med* 48: 983–1001, 2010.
66. **Zimmerman MC, Davisson RL.** Redox signaling in central neural regulation of cardiovascular function. *Prog Biophys Mol Biol* 84: 125–149, 2004.
67. **Zimmerman MC, Dunlay RP, Lazartigues E, Zhang Y, Sharma RV, Engelhardt JF, Davisson RL.** Requirement for Rac1-dependent NADPH oxidase in the cardiovascular and dipsogenic actions of angiotensin II in the brain. *Circ Res* 95: 532–539, 2004.
68. **Zimmerman MC, Lazartigues E, Lang JA, Sinnayah P, Ahmad IM, Spitz DR, Davisson RL.** Superoxide mediates the actions of angiotensin II in the central nervous system. *Circ Res* 91: 1038–1045, 2002.
69. **Zimmerman MC, Lazartigues E, Sharma RV, Davisson RL.** Hypertension caused by angiotensin II infusion involves increased superoxide production in the central nervous system. *Circ Res* 95: 210–216, 2004.
70. **Zimmerman MC, Sharma RV, Davisson RL.** Superoxide mediates angiotensin II-induced influx of extracellular calcium in neural cells. *Hypertension* 45: 717–723, 2005.